

# SIMULATION OF HIGH-TEMPERATURE CORROSION BEHAVIOR OF Ti6Al4V ALLOY IN MARINE ENVIRONMENTS

## SIMULACIJA POTEKA VISOKO TEMPERATURNE KOROZIJE ZLITINE TIPA Ti6Al4V V MORSKEM OKOLJU

Rongtao Zhu<sup>1,2</sup>, Liang Zhang<sup>1\*</sup>, Yuan Bo<sup>1</sup>, Wei Chen<sup>1</sup>, Shilu Chen<sup>1</sup>, Shan Chi<sup>1</sup>, Chunjiang Guo<sup>1</sup>, Zhiwen Xie<sup>2</sup>

<sup>1</sup>Institute of Intelligent Manufacturing Technology, Shenzhen Polytechnic University, Shenzhen 518055, China

<sup>2</sup>School of Mechanical Engineering and Automation, University of Science and Technology Liaoning, Anshan 114051, China

Prejem rokopisa – received: 2024-04-27; sprejem za objavo – accepted for publication: 2024-12-02

doi:10.17222/mit.2024.1172

High-temperature oxidation and corrosion behavior of Ti6Al4V alloy at 650 °C for 1000 h were investigated using a salt mixture (25 w/% NaCl and 75 w/% Na<sub>2</sub>SO<sub>4</sub>) as the thermal corrosion medium. The mass increase due to the alloy's oxidation and thermal corrosion were analyzed quantitatively. The surface morphology and cross-sectional structure of the alloy after oxidation and thermal corrosion were scrutinized and analyzed via X-ray diffraction (XRD), scanning electron microscopy (SEM), and energy dispersive spectroscopy (EDS). Results show that Ti6Al4V alloy exhibits a certain antioxidant property in a high-temperature oxidation environment at 650 °C, but this antioxidant property is gradually weakened with the prolongation of the oxidization time. The synergistic effect of oxygen and hot salt further accelerates the corrosion degradation of the oxide layer of Ti6Al4V alloy in the high-temperature hot-salt environment at 650 °C.

Keywords: Ti6Al4V alloy, high-temperature oxidation, hot-salt test, marine environment

Avtorji v članku opisujejo visoko-temperaturno oksidacijo in korozijsko obnašanje zlitine Ti6Al4V pri njenem zadrževanju na 650 °C za 1000 ur v slani mešanici termalno-korozijskega medija s sestavo 25 w/% NaCl in 75 w/% Na<sub>2</sub>SO<sub>4</sub>. Masa zlitine je naraščala zaradi njene korozije. Avtorji so njeno naraščanje zasledovali in analizirali kvantitativno. Površinsko morfologijo zlitine in njeno mikrostrukturo v preseku so po izvedenih preizkusih analizirali z rentgensko difrakcijo (XRD), vrstično elektronsko mikroskopijo (SEM) in energijsko disperzijsko spektroskopijo (EDS). Rezultati analiz so pokazali, da ima preiskovana zlitina Ti6Al4V določene antioksidantske visoko-temperaturne lastnosti pri 650 °C v izbranem korozijskem okolju. Vendar pa s podaljševanjem časa oksidacije ta odpornost proti koroziji slabi. Sinergijski učinek kisika in vroče soli pospešuje korozijsko degradacijo oksidnega filma na zlitini Ti6Al4V v izbranem, istočasno agresivno slanem in visoko-temperaturnem okolju.

Ključne besede: zlitina Ti6Al4V, visoko-temperaturna oksidacija, vroči slani test, morsko okolje

## 1 INTRODUCTION

As a critical component of an aircraft, the thrust-to-weight ratio of aero engines is a key parameter for evaluating engine performance.<sup>1</sup> Therefore, titanium alloys, with their high specific strength and excellent corrosion resistance, are considered as top candidate materials for aerospace engines.<sup>2-4</sup> However, many components of aero engines operate in harsh service environments characterized by high temperatures, high pressures, high stresses, and high corrosiveness. Components made of titanium alloys are inevitably exposed to high-temperature oxidizing environments during service, resulting in severe oxidative corrosion damage. In extremely harsh high-temperature marine environments, titanium-alloy components form eutectic salt mixtures with low melting points on their surfaces, leading to molten salt corrosion making the material no longer suitable for service re-

quirements.<sup>5-8</sup> Currently, Ti6Al4V, as a typical titanium alloy with an ( $\alpha+\beta$ ) two-phase structure, is widely used due to its lightweight, high strength, non-magnetic properties, and excellent biocompatibility.<sup>9-11</sup> Consequently, a comprehensive investigation into the corrosion damage behavior and degradation mechanism of Ti6Al4V alloy under high-temperature marine environments holds significant theoretical value and practical engineering implications.

In recent years, numerous researchers have conducted investigations into the corrosion damage behavior of titanium alloys within high-temperature and hot-salt environments.<sup>12-16</sup> Casadebaigt et al.<sup>12</sup> reported that Ti6Al4V alloy forms an oxide layer with TiO<sub>2</sub> and Al<sub>2</sub>O<sub>3</sub> as the main components at 500–600 °C and has good antioxidant properties. Guleryuz et al.<sup>13</sup> reported the antioxidant properties of Ti6Al4V alloy at temperatures above 600 °C. With the increase in the temperature, the pores of the oxide layer, which is mainly composed of TiO<sub>2</sub> and Al<sub>2</sub>O<sub>3</sub>, gradually increased, and even rupture and spalling occurred on the surface. Subsequently, to explore the effects of a marine environment on TiAl alloys,

\*Corresponding author's e-mail:  
zhangliang@szpu.edu.cn (Liang Zhang)



© 2024 The Author(s). Except when otherwise noted, articles in this journal are published under the terms and conditions of the Creative Commons Attribution 4.0 International License (CC BY 4.0).

Li et al.<sup>14</sup> investigated the corrosion resistance of Ti6Al4V alloy that decreased with the increasing grain size in a high-concentration NaCl solution (15 w%). The better quality of the protective film on the surface of the fine grains hindered further dissolution of the alloy. Zhao et al.<sup>15</sup> reported that the oxidation of titanium alloys in a molten-salt corrosion environment (25 w% NaCl + 75 w% Na<sub>2</sub>SO<sub>4</sub>) was significantly accelerated. The corroded surface was loose and porous and there was poor adhesion between the oxide layer and the substrate. M. Mitoraj-Królikowska et al.<sup>16</sup> reported the corrosion damage of Ti-Al alloys within hot-salt environments. It was revealed that sodium chloride in aerosols over the oceans reacts with sulfur oxides produced by the combustion of aero-engine fuels to form sodium sulfate deposits on the surfaces of aero-engine hot-end components, leading to severe thermal corrosion and a significant reduction in the service life of the material. Obviously, the oxidation and degradation reactions of titanium alloys exposed to a marine environment are also affected by hot-salt corrosion.

In this study, high-temperature oxidation and high-temperature hot-salt corrosion tests were designed to simulate the service environment of Ti6Al4V alloy in the ocean. The oxidative degradation mechanisms of Ti6Al4V alloys from two environments were compared in detail by analyzing the material and morphological changes of the oxide layer at different stages of the two sets of tests. The effects of volatile chlorides and non-protective corrosion products, generated by NaCl and Na<sub>2</sub>SO<sub>4</sub>, on the oxidative corrosion were discussed in detail.

## 2 MATERIALS AND METHODS

### 2.1 Preparation of the materials

The experimental material in this study was a standard ( $\alpha+\beta$ )-type alloy, known as Ti6Al4V (Shenzhen Si Rui Additive Liability Co., LTD). The alloy underwent preparation to form square block samples measuring (15 × 15 × 5) mm via wire-cutting. Surface treatment involved sanding with 180 mesh, 320 mesh, and 600 mesh SiC sandpaper, followed by ultrasonic cleaning in anhydrous ethanol at 50 °C for 20 min to eliminate surface contaminants. Subsequently, the samples were dried and stored for subsequent use. A detailed composition of the Ti6Al4V alloy is presented in **Table 1**.

**Table 1:** Chemical composition of the original sample (w%)

Al	V	Fe	C	O	N	Ti
5.5–6.8	3.5–4.5	≤0.3	≤0.1	≤0.2	≤0.05	Bal.

### 2.2 Experimental design

A high-temperature oxidation test and hot-salt test were carried out in a muffle furnace. The high-temperature oxidation test involves placing the sample in a cruci-

ble (Al<sub>2</sub>O<sub>3</sub>) and subsequently placing the crucible with the specimen in a muffle furnace for oxidation. The high-temperature thermal salt test is based on the high-temperature oxidation test, in which the surface of the sample is coated with a mixed salt solution of (25 w% NaCl + 75 w% Na<sub>2</sub>SO<sub>4</sub>). To ensure the uniformity of the salt film on the surface of the samples, the salt addition treatment was carried out several times to ensure that the salt content of the samples was 3–5 mg/cm<sup>2</sup>. The temperature and heating rate for the above tests were 650 °C and 10 °C/min, respectively. The duration of the test was 1000 h. The muffle furnace was air-cooled every 20 h and after cooling to room temperature, the crucible with the samples was weighed for mass change using an electronic balance with an accuracy of 10<sup>-4</sup> g. To avoid mass deviation caused by residual salt, Sample M2 was washed with boiling deionized water for 20 min before weighing. To reduce the experimental variation error, both Sample M1 and M2 were measured using three sets of parallel samples, and the average mass was used as the final result. The specific experimental design is shown in **Table 2**.

**Table 2:** Details of experimental design for Ti6Al4V alloy

Sample	Test type	Time
M0	Original sample	–
M1	High-temperature oxidation test	1000 h
M2	High-temperature hot-salt test	1000 h

### 2.3 Test and analysis

X-ray diffraction (XRD, X' Pert Powder, PANalytical B.V., Almelo, Netherlands) was used to characterize the surface phase compositions of the samples after the above tests, with a radiation source of Cu-K $\alpha$ , a scanning range of 10–90°, and a scanning time of 2 min. The surface and cross-section images of Samples M1 and M2 after corrosion were characterized using scanning electron microscopy (SEM, Zeiss  $\Sigma$  IGMA HD, Carl Zeiss, Jena, Germany). This was combined with an energy dispersive spectrometer (EDS) to further determine the local elemental composition and specific distribution on the surface and cross-section of the test samples.

## 3 RESULTS

### 3.1 Corrosion kinetic curve

**Figure 1** shows the weight gain curves of Samples M1 and M2 after exposure to oxidizing and hot-salt environments for 1000 h. Sample M1 shows a continuous and stable mass-growth trend in the pre-test period. Its slope of the oxidation kinetic curve gradually slows down with the increase in the oxidation time, reaching 4.32 mg/cm<sup>2</sup> at 700 h, indicating that Ti6Al4V has a good antioxidant property in the pre-test period of the oxidation test. However, as the oxidation test continues, the oxidation weight gain curve undergoes a significant

decrease and then it rises again, reaching  $5.03 \text{ mg/cm}^2$  at 1000 h, indicating that the oxidized layer appears to be peeling off and the matrix is further oxidized. In contrast, Sample M2 exhibits a more pronounced initial mass change during hot-salt corrosion. After 80 h of the hot-salt test, the mass rapidly increases by  $4.59 \text{ mg/cm}^2$ , indicating an accelerated growth rate of the oxide layer in the hot-salt corrosion environment. Subsequently, the curves exhibit fluctuating patterns, suggesting an accelerated rate of oxide-layer degradation and failure in the hot-salt environment, leading to shedding and regeneration of the oxide layer on the alloy surface during the pre-test period. After 1000 h of hot-salt corrosion, the weight gain of Sample M2 is significantly lower than that of Sample M1, measuring  $3.12 \text{ mg/cm}^2$ .

### 3.2 Surface macroscopic morphology

**Figure 2** shows the surface macroscopic morphology of Samples M1 and M2 at various time points. As shown in **Figures 2a** to **2c**, the surface of Sample M1 in the pre- and mid-term periods before the oxidation test shows an obvious earthy yellow color, consistent with the typical characteristics of a  $\text{TiO}_2$  oxide layer. The surface morphology is intact, without significant oxidative corrosion.<sup>12</sup> **Figure 2d** shows the macroscopic morphology of the surface of Sample M1 after oxidation for 1000 h. It is observed that the integrity of the surface oxide layer is damaged, and cracking, or even detachment, occurs. In contrast, numerous minute depressions are observed in the oxide layer on the surface of Sample M2 following the 100-h hot-salt test (**Figure 2e**). Progressing through the test, **Figure 2f** shows that the oxide layer of Sample M2 begins to deteriorate after 200 h, leading to the oxide layer separation from the substrate. Subsequently, as shown in **Figure 2g**, after 400 h of the hot-salt test, Sample M2 exhibits a worsening corrosion trend, with the separation gap further widening. The bonding strength

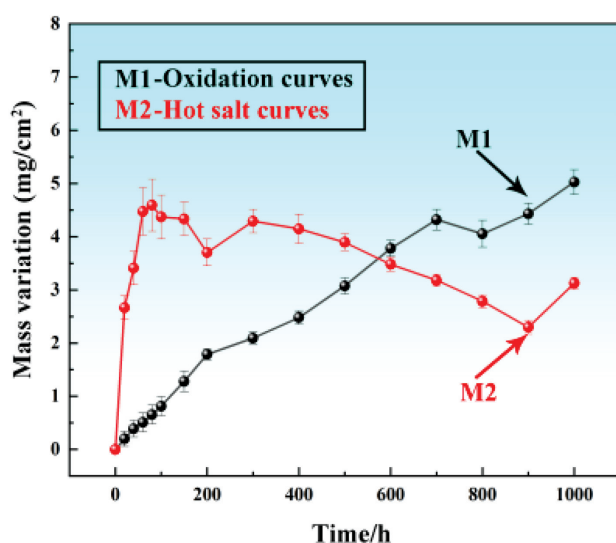


**Figure 1:** Corrosion kinetics of Samples M1 and M2

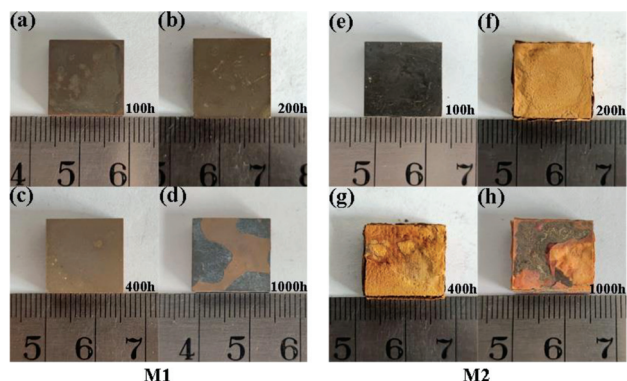


**Figure 2:** Surface macroscopic morphology of Samples M1 and M2 at various times: a) M1 100 h, b) M1 200 h, c) M1 400 h, d) M1 1000 h, e) M2 100 h, f) M2 200 h, g) M2 400 h, h) M2 1000 h

between the oxide layer and the substrate significantly decreases, accompanied by the formation of numerous corrosion pits on the surface. Finally, as shown in **Figure 2h**, following 1000 h of corrosion, the surface oxide layer exhibits extensive cracking and detachment, resulting in the degradation of the internal matrix due to corrosion.

### 3.3 XRD phase composition

**Figure 3** presents the surface XRD physical phase analysis of Samples M1 and M2 after oxidation at  $650^\circ\text{C}$  and a 1000-h hot-salt test. As shown in **Figure 3a**, the primary products resulting from the oxidation of Sample M1 at  $650^\circ\text{C}$  are  $\text{TiO}_2$  and  $\text{Al}_2\text{O}_3$ . Other oxides, such as  $\text{V}_2\text{O}_5$ , do not exhibit distinct diffraction peaks, which can be attributed to the low V content in the alloy. In contrast, as shown in **Figure 3b**, Sample M2 displays non-protective corrosion products, including  $\text{Na}_2\text{TiO}_3$  and  $\text{NaAlO}_2$ , alongside the oxides observed in M1 under the hot-salt conditions at  $650^\circ\text{C}$ . This observation suggests that the hot-salt environment triggers the formation of non-protective corrosion products, contributing to accelerated degradation and potential failure of the oxide layer.<sup>21</sup>

### 3.4 Surface micro-morphology and composition

**Figure 4** shows the surface SEM morphology and corresponding EDS patterns of Samples M1 and M2 after 100 h of testing. As shown in **Figure 4a**, the surface of Sample M1 remains intact and dense after undergoing a 100-h oxidation test, with visible scratches resulting from polishing on the surface of the oxide layer. The surface morphology, as shown in **Figure 4b** at a higher magnification, primarily appears in the form of long fibers, consistent with the microstructural morphology of Ti element under oxidation conditions.<sup>17</sup> Furthermore, the EDS energy spectrum shown in **Figure 4c** confirms that the surface products mainly consist of  $\text{TiO}_2$ . In contrast, Sample M2, as shown in **Figure 4d**, exhibits a

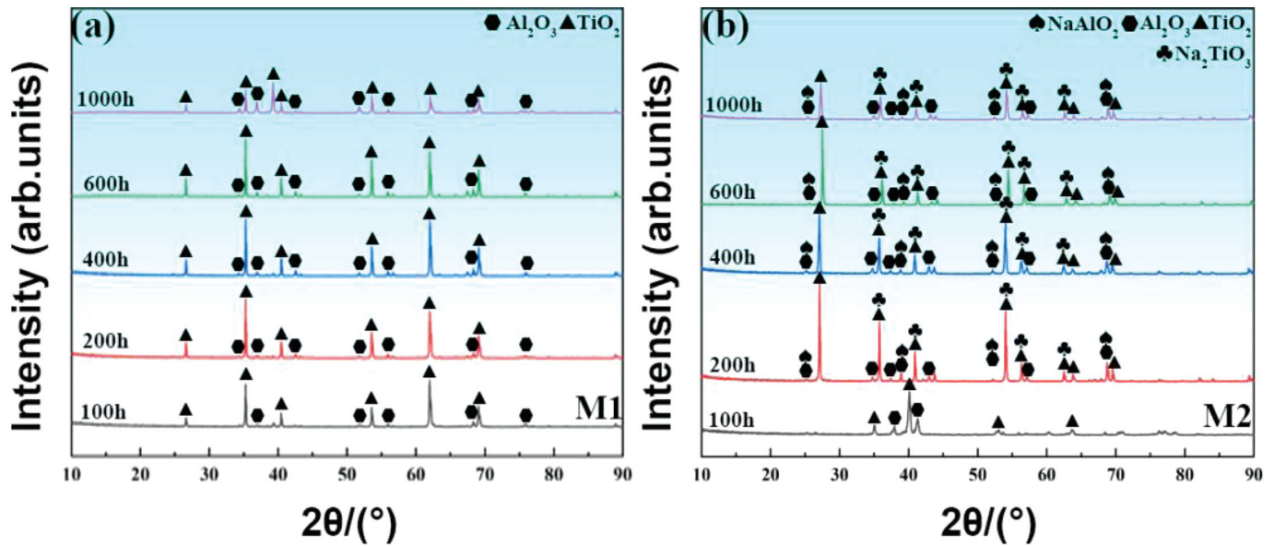


Figure 3: XRD analysis of Samples M1 and M2 at different times: a) Sample M1, b) Sample M2

large number of micro-holes on its surface after 100 h of hot-salt corrosion, indicating potential corrosion degradation of the surface oxide layer. Figure 4e shows a locally enlarged image where the holes on the surface are even more apparent after hot-salt corrosion, resulting in a thinner and less dense oxide layer. Moreover, a cluster-like morphology replaces the long fiber morphology after hot-salt corrosion, indicating an aggravated degradation of the surface due to the corrosive effect of the hot-salt environment.

Figure 5 shows the surface SEM morphology and corresponding EDS patterns of Samples M1 and M2 af-

ter 400 h of testing. As shown in Figure 5a, the surface of Sample M1 remains relatively intact after 400 h of oxidation testing. However, the surface oxide scales are thickened, and the original wear scratches induced by sandpaper are no longer visible. Granular structures are observed on the surface in addition to the long fibers, as shown in Figure 5b. The EDS energy spectrum shown in Figure 5c indicates that the oxide layer predominantly consists of TiO<sub>2</sub> and Al<sub>2</sub>O<sub>3</sub> at this stage. This finding suggests that the Ti element in Ti6Al4V indicates a preferential reaction with O<sub>2</sub>, while the Al element in the alloy only reacts with O<sub>2</sub> as the oxidation time increases<sup>14</sup>.

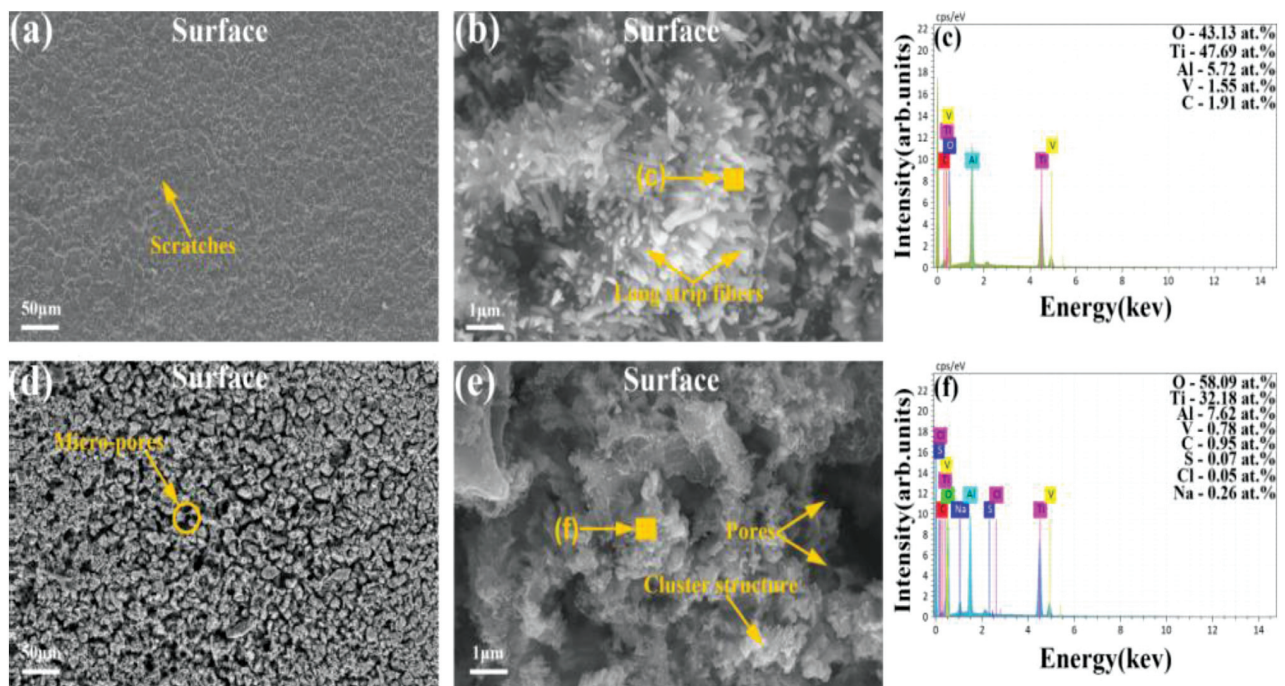
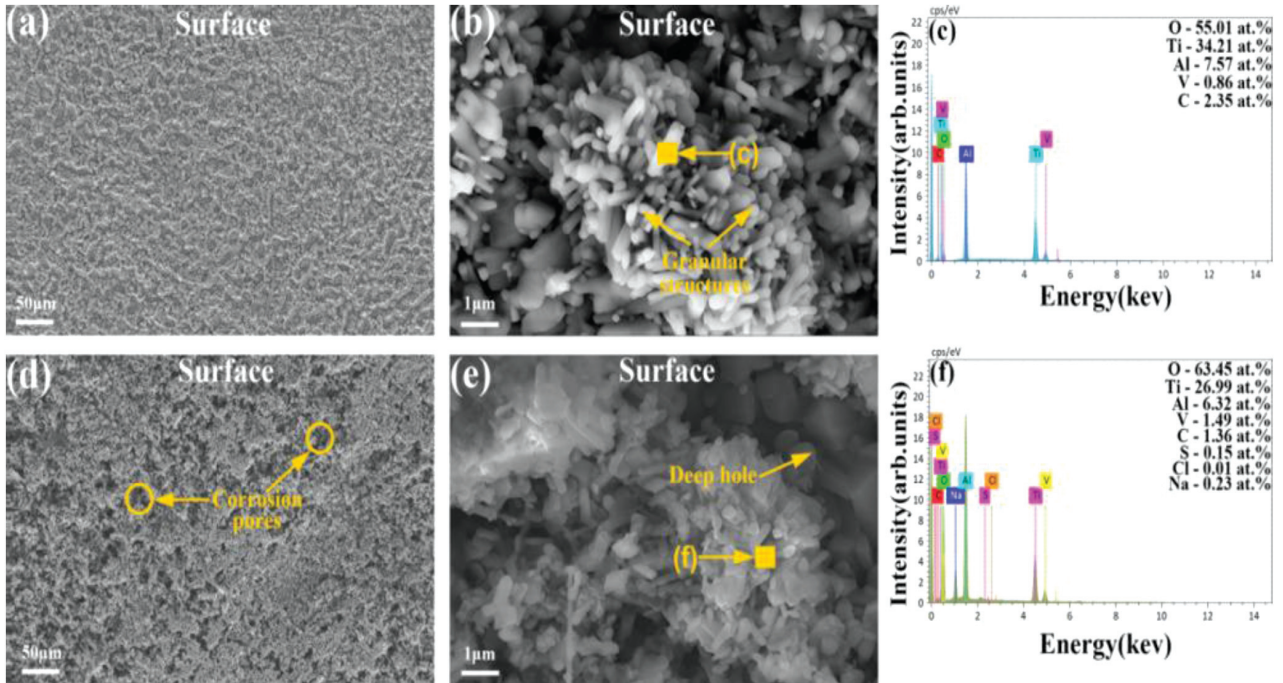


Figure 4: Surface SEM morphology and corresponding EDS patterns of Samples M1 and M2 after 100 h of testing: a)–c) Sample M1, d)–f) Sample M2



**Figure 5:** Surface SEM morphology and corresponding EDS patterns of Samples M1 and M2 after 400 h of testing: a)–c) Sample M1, d)–f) Sample M2

In contrast, the micro-pores on the surface of Sample M2 in **Figure 5d** undergo further corrosion after 400 h of hot-salt corrosion, causing the pores to interconnect and form large-area corrosion pits on the surface. **Figure 5e** shows a locally magnified image that reveals an increase in the number of corrosion holes on the surface, with the vertical depth of the holes further deepening.

**Figure 6** shows the surface SEM morphology and corresponding EDS patterns of Samples M1 and M2 after 1000 h of testing. As shown in **Figure 6a**, crack forming and shedding are observed on the surface of Sample M1 after 1000 h of oxidation testing. This proves that with the increase in the oxidation time, there is a tendency for a gradual destruction of the Ti6Al4V sur-

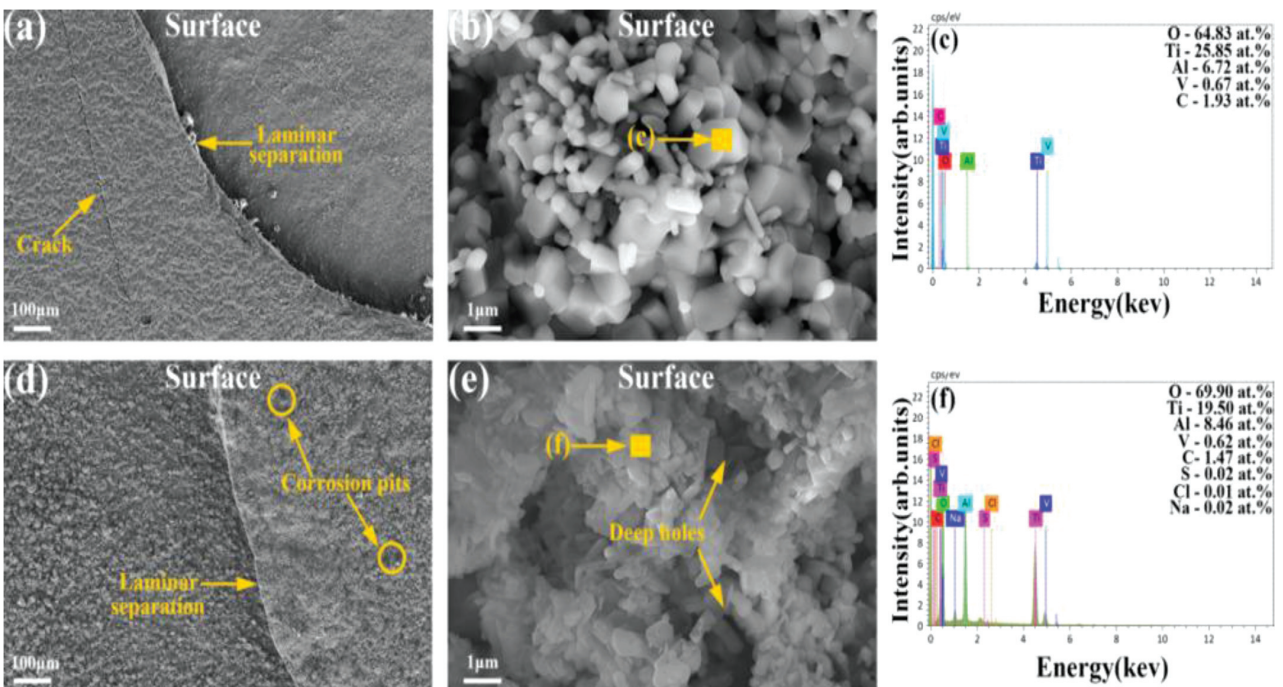


**Figure 6:** Surface SEM morphology and corresponding EDS patterns of Samples M1 and M2 after 1000 h of testing: a)–c) Sample M1, d)–f) Sample M2

face oxide layer, which eventually leads to the failure of the oxide layer. Combined with **Figure 6b** and **6c**, it becomes apparent that upon the removal of the oxide layer, the substrate is once again exposed to high temperatures, initiating renewed oxidation reactions with oxygen and resulting in the formation of a new oxide layer on the surface. As shown in **Figure 6d**, after 1000 hours of hot-salt testing, Samples M2 and M1 show the same oxide layer peeling. The corrosion shedding of Sample M2 is more serious, and a large corrosion pit is formed on the surface of the un-shedded oxide layer, exposing the substrate that is unprotected by an oxide layer to a hot salt environment. In comparison to high-temperature oxidation conditions, hot-salt corrosion significantly accelerates the degradation of the surface substrate and leads to the formation of corrosion pits on the exposed surface, resembling those observed in the early stages of hot-salt experiments. This indicates that the surface structural damage and corrosion degradation rate of the Ti6Al4V

alloy oxidation products are exacerbated in the hot-salt environment.

### 3.5 Cross-section micro-morphology and element distribution

**Figure 7** shows the cross-sectional SEM morphology and corresponding EDS patterns of Sample M1 after the oxidation test. As shown in **Figure 7a**, a clear bilayer structure with good bonding between the interfaces is observed in Sample M1 after 100 h of oxidation testing. The oxidized layer exhibits excellent densification and integrity without transverse or longitudinal crack formation, and its thickness is about 23  $\mu\text{m}$ . Combined with the EDS pattern from **Figure 7b**, it shows that the main product of the oxide layer is  $\text{TiO}_2$ . A small amount of  $\text{Al}_2\text{O}_3$  is detected on the surface of the oxide layer, while an obvious upward diffusion of the underlying Al element occurs. As shown in **Figure 7c**, tiny transverse

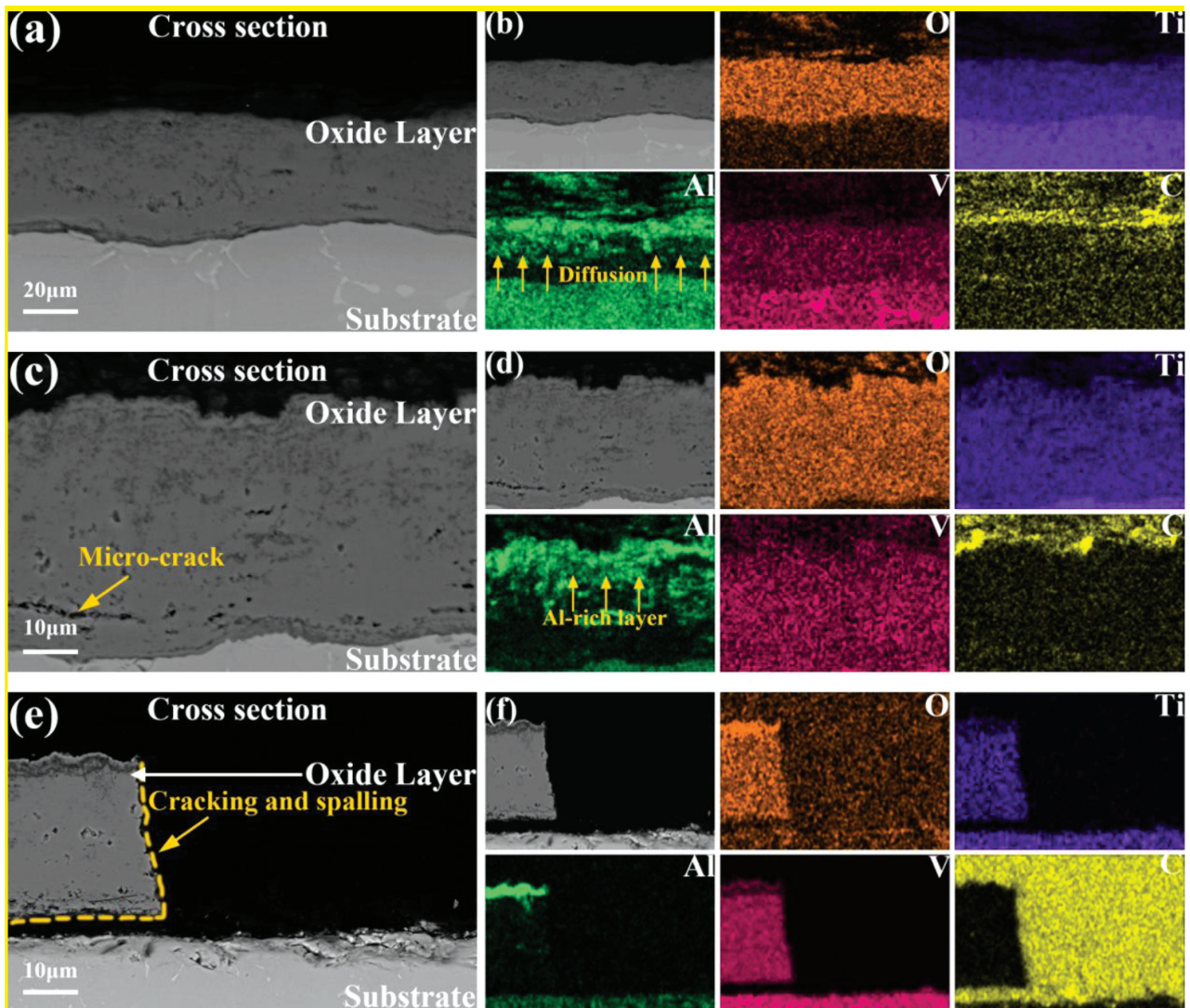


**Figure 7:** Cross-sectional SEM morphology and corresponding EDS patterns of Sample M1 after oxidation testing: a), b) 100 h, c), d) 400 h, e), f) 1000 h

cracks formed inside the oxide layer after 400 h of oxidation testing, but the thickness of the oxide layer did not change significantly, proving that the oxide layer effectively prevented oxygen from further eroding the substrate. Combined with **Figure 7d**, it shows that Ti and Al elements are mainly detected on the surface at this point, and Al elements show obvious diffusion enrichment in the outermost part of the surface layer. As shown in **Figure 7e**, cracking occurs between the oxide layer and the substrate after 1000 h of oxidation testing, and longitudinal cracks appear throughout the oxide layer, resulting in

the detachment of a part of the oxide layer. It is further demonstrated that the Ti6Al4V alloy gradually degrades the oxide layer and loses its protective effect as the oxidation time increases.

**Figure 8** shows the cross-sectional SEM morphology and corresponding EDS patterns of Sample M2 after the hot-salt test. As shown in **Figure 8a**, a large number of corrosion holes are observed on the surface of Sample M2 after 100 h of hot-salt testing, showing a tendency of extending downward. Combined with the cross-sectional SEM image from **Figure 8b**, it is shown that O<sub>2</sub> diffuses

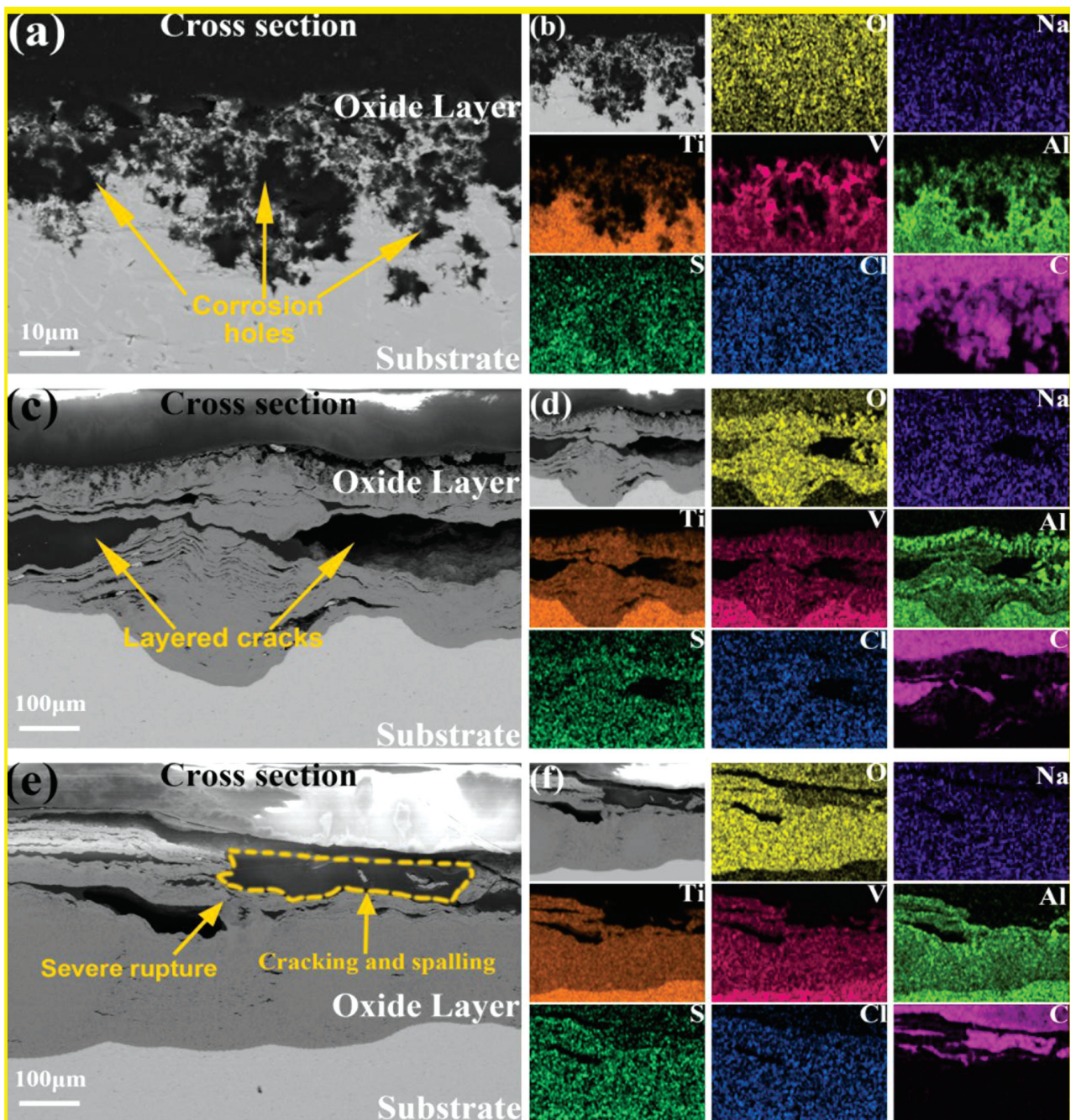


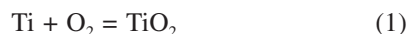
**Figure 8:** Cross-sectional SEM morphology and corresponding EDS patterns of Sample M2 after the hot-salt test: a), b) 100 h, c) d) 400 h, e), f) 1000 h

downward along the corrosion holes, and the substrate is subjected to an extensive oxidative attack. As shown in **Figure 8c**, the thickness of the oxide layer after 400 h of hot-salt corrosion is as high as 221  $\mu\text{m}$ , which is far more than the thickness of oxidative erosion. At the same time, a large number of transverse cracks form on the surface oxide layer, leading to the interlayer separation of cracks combining with each other as the cracks expand further. Combined with the EDS pattern from **Figure 8d** and the XRD analysis from **Figure 3**, it shows that mixed salt leads to the emergence and growth of non-protective corrosion products, which are the reason for further thickening of the oxide layer and a looser structure. As shown in **Figure 8e**, the shedding of the oxide layer after 1000 h of hot salt corrosion occurs at a deeper vertical scale than that of the oxidation test. Moreover, once shedding occurs, it initiates a cycle of further shedding due to the persistent interlayer separation within the oxide layer. This further demonstrates that the surface structure damage and the corrosion degradation rate of some of the oxidation products of Ti6Al4V alloys are exacerbated in a hot-salt environment.

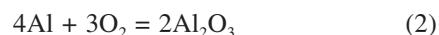
#### 4 DISCUSSION

**Figure 9** shows the corrosion and degradation mechanism of Ti6Al4V alloy during an oxidation test at 650  $^{\circ}\text{C}$ . As shown in **Figure 9a**, Sample M1 underwent an oxidation reaction on the surface of the alloy during the initial stage of the test. The standard Gibbs free energies of the elements in Ti6Al4V reacting with 1 mol  $\text{O}_2$  to form the corresponding oxides are:  $\Delta G^0 \text{Al}_2\text{O}_3$  ( $-902 \text{ KJ/mol}$ )  $<$   $\Delta G^0 \text{TiO}_2$  ( $-759 \text{ KJ/mol}$ )  $<$   $\Delta G^0 \text{V}_2\text{O}_5$  ( $-144 \text{ KJ/mol}$ ), respectively. Therefore, thermodynamically,  $\text{Al}_2\text{O}_3$  is formed more preferentially than  $\text{TiO}_2$  and  $\text{V}_2\text{O}_5$ , but the formation of oxides is not only determined by thermodynamics, but also the kinetics of oxide-growth needs to be considered. Since  $\text{TiO}_2$  has much higher growth kinetics than  $\text{Al}_2\text{O}_3$ ,<sup>18,19</sup> Therefore, according to Equation (1),  $\text{O}_2$  reacts preferentially with Ti to produce  $\text{TiO}_2$ , but the continuous oxidation reaction continuously consumes Ti in the surface layer of the alloy, leading to a depletion of Ti at the junction of the  $\text{TiO}_2$

oxidized layer and the matrix. This causes the aggregation of Al at this place, forming an aluminum-rich layer.



As shown in **Figure 9b**, as the oxidation test proceeds, the  $\text{TiO}_2$  oxide layer exhibits high growth stress because it is a brittle product. As the oxidation test proceeds, the oxide layer develops tiny cracks, resulting in a less dense structure. As a result, the Al element diffuses upwards and is enriched on the surface of the sample through the  $\text{TiO}_2$  layer. When it is in contact with external oxygen, a continuous and dense  $\text{Al}_2\text{O}_3$  layer is rapidly formed on the outside of the  $\text{TiO}_2$  oxide layer as shown by Equation (2).<sup>20</sup> Meanwhile, according to Equation (3), element V reacts with  $\text{O}_2$  to form a small amount of  $\text{V}_2\text{O}_5$ . With the continuous formation of oxidation products, the thickness of the oxide layer is gradually increased, and the downward diffusion rate of  $\text{O}_2$  is gradually slowed down, resulting in a slowdown of the matrix oxidation rate. This is the reason why the slope of the oxidation weight-gain curve in **Figure 1** decreases gradually with time.



As shown in **Figure 9c**, as the oxidation test continued, thermal fatigue cracks formed at the junction of the oxide layer and the substrate due to thermal stresses arising from the differing coefficients of thermal expansion of  $\text{TiO}_2$ ,  $\text{Al}_2\text{O}_3$ , and the Ti6Al4V alloy, which were  $8.2 \times 10^{-6}/\text{K}$ ,  $8.1 \times 10^{-6}/\text{K}$  and  $10 \times 10^{-6}/\text{K}$ , respectively.<sup>21</sup> The cracks continued to extend with the oxidation time and eventually led to the interlayer separation and localized detachment.

**Figure 10** shows the corrosion process and degradation mechanism of Ti6Al4V alloy during a hot-salt test at 650  $^{\circ}\text{C}$ . As shown in **Figure 10a**, Sample M2 accelerated the oxidation reaction at the initial stage of the test due to the corrosive effect of the salt film, and a composite oxide layer ( $\text{TiO}_2$ ,  $\text{Al}_2\text{O}_3$ ,  $\text{V}_2\text{O}_5$ ) was formed rapidly on the alloy surface in accordance with Equations (1)–(3). The corrosive effect of the salt film occurred because the salt mixture (25 w/% NaCl + 75 w/%  $\text{Na}_2\text{SO}_4$ ) was molten at 650  $^{\circ}\text{C}$  and it was capable of eutectic reactions, producing sulfide and  $\text{Cl}_2$ .<sup>22–24</sup> as follows:

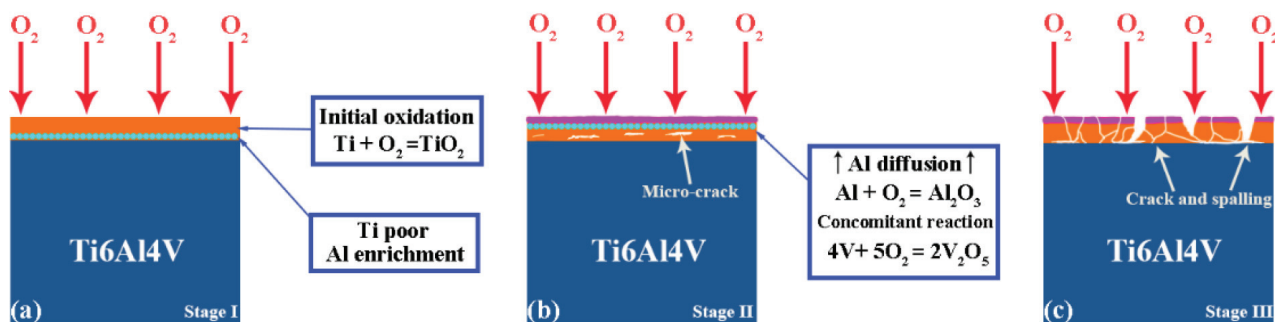
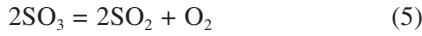
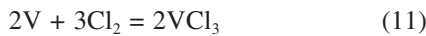


**Figure 9:** Corrosion damage mechanism diagram of high-temperature oxidation test: a) Stage I, b) Stage II, c) Stage III

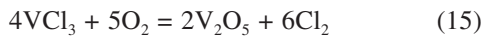
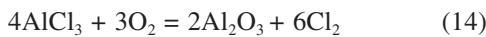
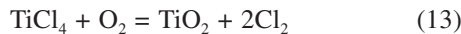
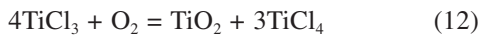


The  $\text{Cl}_2$  generated with the above reaction diffuses downward at the interface between the molten salt film and the oxide layer, generating the corresponding chlorides with Ti, Al, and V.<sup>25</sup> The specific reactions are as follows:



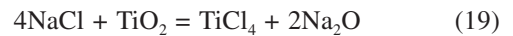
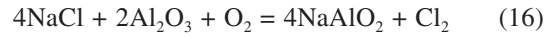
Due to its high volatility in high-temperature environments, chloride leads to the formation of numerous corrosion holes within the oxide layer. As a result, the overall integrity of the oxide layer is compromised, which explains the rapid increase and subsequent decrease in the oxidized weight gain curve of Sample M2 as shown in **Figure 1**.

As shown in **Figure 10b**, as the hot-salt test proceeds, a large number of holes form due to the aggregation effect. These provide a channel for inward diffusion of the molten salt and  $\text{O}_2$ , allowing  $\text{O}_2$  to come into contact with chloride and generate the corresponding oxidation products in accordance with Equations (12)–(15).<sup>26</sup>



It is evident that  $\text{Cl}_2$  serves as a crucial carrier in the aforementioned reaction, thereby expediting the formation of the oxide layer to a thickness significantly greater than that observed in simultaneous oxidation tests. At the same time, as the composite oxide layer exhibits high growth stress, the stress in the oxide layer is uneven and cracks form. Combined with the mismatch of thermal ex-

pansion coefficients, this leads to the generation of interlayer separation. In addition,  $\text{NaCl}$  exacerbates the degradation rate of  $\text{Al}_2\text{O}_3$  and  $\text{TiO}_2$ , generating non-protective corrosion products such as  $\text{NaAlO}_2$  and  $\text{Na}_2\text{TiO}_3$  in accordance with Equations (16)–(19).<sup>27</sup> These corrosion products further intensify segregation within the oxide layer, consequently altering its internal structure.



As shown in **Figure 10c**, the longitudinal cracks continued to expand and extend as the hot-salt test progressed. The thermal stresses generated within the oxide layer, due to brittle stresses and differences in coefficients of thermal expansion, resulted in significant damage to the surface integrity and large-scale detachment of the oxide layer. The substrate, corroded by the hot-salt environment and covered with a thick oxide layer, only shedded its external oxide layer. After the oxide layer was detached, the remaining oxide layer struggled to resist the corrosion of molten salt and oxygen, causing the substrate to repeat the above reaction process.

In this study, it was determined that the Ti6Al4V alloy does not exhibit long-term resistance to oxidation and hot-salt corrosion at 650 °C. To improve the service capability of the Ti6Al4V alloy under high temperature and in hot-salt environments, future research will focus on utilizing laser cladding to apply coatings on the surface of the Ti6Al4V alloy. This process aims to improve surface densification, reduce the rate of oxygen infiltration, and mitigate the corrosion and erosion caused by molten salt.

## 5 CONCLUSIONS

In this study, the high-temperature damage behavior and degradation mechanism of the Ti6Al4V alloy kept for a long period in a marine environment were researched systematically using a high-temperature oxida-

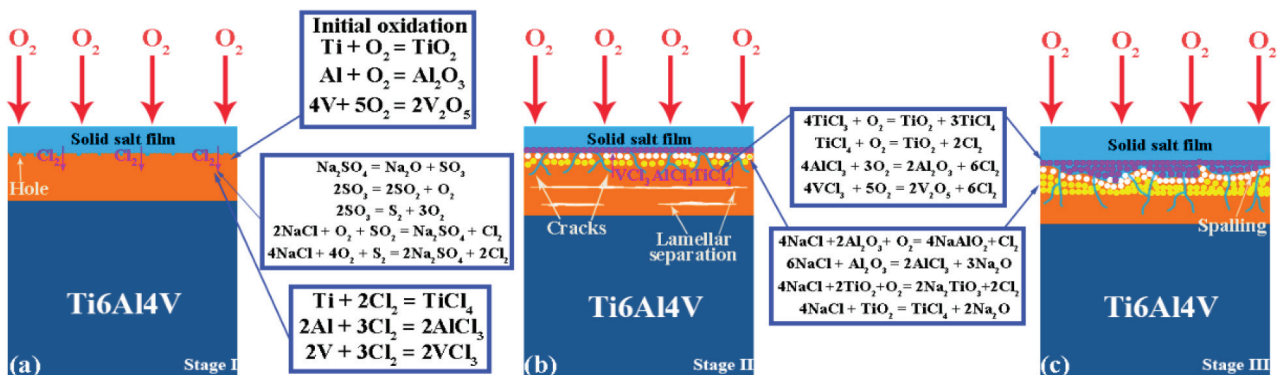


**Figure 10:** Corrosion damage mechanism diagram of high-temperature hot-salt test: a) Stage I, b) Stage II, c) Stage III

tion test and high-temperature hot-salt corrosion test. The main conclusions are as follows:

(1) The Ti6Al4V alloy showed favorable antioxidant properties during short-term high-temperature oxidation tests, and the generated oxidation products were mainly  $\text{TiO}_2$  and  $\text{Al}_2\text{O}_3$ . However, during the long-term oxidation test, the brittle and thermal stresses in the oxide layer led to gradual cracking of the oxide layer. As the cracks continued to extend, the oxide layer eventually fell off.

(2) The Ti6Al4V alloy was exposed to both oxygen and molten salt corrosion during the high-temperature hot-salt test, which accelerated the degradation rate of the oxide layer. The  $\text{Cl}_2$  generated by the eutectic reaction of mixed salts maintained its own cyclic reaction, and the formation of volatile chlorides and non-protective corrosion products ( $\text{NaAlO}_2$ ,  $\text{Na}_2\text{TiO}_3$ ) further destroyed the structural density of the oxide layer, leading to severe delamination.

### Acknowledgment

This work was supported by Research Projects of the Department of Education of Guangdong Province (2024ZDZX3080), and the Shenzhen Polytechnic University (602331004PQ, 6021320035K, and 6024310028K).

### 6 REFERENCES

- J. M. Cai, C. X. Cao, Alloy Design and Application Expectation of a New Generation 600 °C High Temperature Titanium Alloy, *J. Aeronaut. Mater.*, 34 (2014) 4, 27–36, doi:10.11868/j.issn.1005-5053.2014.4.002
- K. Zhang, Z. W. Li, W. Gao, Hot corrosion behaviour of Ti–Al based intermetallics, *Mater. Lett.*, 57 (2002) 4, 834–843, doi:10.1016/S0167-577X(02)00882-0
- X. X. Ma, Y. D. He, J. P. Lin, D. Wang, J. Zhang, Effect of a magnetron sputtered ( $\text{Al}_2\text{O}_3\text{--Y}_2\text{O}_3$ )/(Pt–Au) laminated coating on hot corrosion resistance of 8Nb–TiAl alloy, *Surf. Coat. Technol.*, 206 (2012) 10, 2690–2697, doi:10.1016/j.surfcoat.2011.11.028
- T. Kitashima, T. Hara, Y. Yang, Y. Hara, *Mater. Des.*, 137 (2018) 5, 355–360, doi:10.1016/j.matdes.2017.10.043
- A. Evstifeev, N. Kazarinov, Y. Petrov, L. Witekx, A. Bednarz, *Eng. Failure Anal.*, 87 (2018), 15–21, doi:10.1016/j.engfailanal.2018.01.006
- Z. Cao, L. Sun, Q. Cao, *Adv. Mat. Res.*, 233–235 (2011), 2409–2412, doi:10.4028/www.scientific.net/AMR.233-235.2409
- M. W. Reedy, T. J. Eden, J. K. Potter, D. E. Wolfe, *Surf. Coat. Technol.*, 206 (2011) 2–3, 464–472, doi:10.1016/j.surfcoat.2011.07.063
- L. Swadźba, B. Formanek, H. M. Gabriel P. Liberski, P. Podolski, Erosion- and Corrosion-Resistant Coatings for Aircraft Compressor Blades, *Surf. Coat. Technol.*, 62 (1993) 1–3, 486–492, doi:10.1016/0257-8972(93)90288-Y
- L. Shao, G. L. Xie, X. H. Liu, W. Yuan, J. B. Yu, Z. H. Hao, W. R. Lu, X. Liu, Combustion behaviour and mechanism of TC4 and TC11 alloys, *Corros. Sci.*, 168 (2020) 15, 108564, doi:10.1016/j.corsci.2020.108564
- H. L. Du, P. K. Datt, D. B. Lewis, J. S. Burnell-Gray, Air Oxidation of Ti6Al4V Alloy between 650 and 850 °C, *Corros. Sci.*, 36 (1994) 4, 631–642, doi:10.1016/0010-938X(94)90069-8
- J. W. Liu, Q. D. Sun, C. A. Zhou, X. B. Wang, H. Li, K. Guo, J. Sun, *Mater. Sci. Eng.*, 766 (2019) 24, 138319, doi:10.1016/j.msea.2019.138319
- A. Casadebaigt, J. Hugues, D. Monceau, High temperature oxidation and embrittlement at 500–600 °C of Ti-6Al-4V alloy fabricated by Laser and Electron Beam Melting, *Corros. Sci.*, 175 (2020), 108875, doi:10.1016/j.corsci.2020.108875
- H. Guleryuz, H. Cimenoglu, Oxidation of Ti-6Al-4V alloy, *J. Alloys Compd.*, 472 (2009) 1–2, 241–246, doi:10.1016/j.jallcom.2008.04.024
- J. Q. Li, X. Lin, P. F. Guo, M. H. Song, W. D. Huang, Electrochemical behaviour of laser solid formed Ti-6Al-4V alloy in a highly concentrated NaCl solution, *Corros. Sci.*, 142 (2018), 161–174, doi:10.1016/j.corsci.2018.07.023
- W. Zhao, B. Xu, Y. Ma, S. Gong, Inter-phase selective corrosion of  $\gamma$ -TiAl alloy in molten salt environment at high temperature, *Prog. Nat. Sci.: Mater. Int.*, 21 (2011) 4, 322–329, doi:10.1016/S1002-0071(12)60064-1
- M. Mitoraj-Królikowska, E. Godlewska, Hot corrosion behaviour of ( $\gamma + \alpha_2$ )-Ti-46Al-8Nb (at.%) and  $\alpha$ -Ti-6Al-1Mn (at.%) alloys, *Corros. Sci.*, 115 (2016), 18–29, doi:10.1016/j.corsci.2016.11.006
- Y. H. Qian, X. C. Li, M. S. Li, J. J. Xu, B. Lu, Hot corrosion of modified  $\text{Ti}_3\text{Al}$ -based alloy coated with thin  $\text{Na}_2\text{SO}_4$  film at 910 and 950 °C in air, *Trans. Nonferrous Met. Soc. China*, 27 (2017) 4, 954–961, doi:10.1016/S1003-6326(17)60111-0
- J. J. Dai, J. Y. Zhu, C. Z. Chen, F. Weng, High temperature oxidation behavior and research status of modifications on improving high temperature oxidation resistance of titanium alloys and titanium aluminides: A review, *J. Alloys Compd.*, 685 (2016), 784–798, doi:10.1016/j.jallcom.2016.06.212
- Y. Garip, Investigation of isothermal oxidation performance of TiAl alloys sintered by different processing methods, *Intermetallics*, 127 (2020), 106985, doi:10.1016/j.intermet.2020.106985
- F. Omidbakhsh, A. R. Ebrahimi, S. H. Mousavi, R. A. Khosroshahi, S. Nazarpour, Effect of oxygen boost diffusion treatment on fatigue behavior of Ti-4Al-2V alloy, *Surf. Coat. Technol.*, 205 (2011) 8–9, 2954–2963, doi:10.1016/j.surfcoat.2010.11.004
- E. Aghion, I. Guinguis, J. Goldman, Corrosion Behavior of Nano/Sub-Micron F401 Titanium Alloy, *Adv. Eng. Mater.*, 17 (2015) 5, 626–631, doi:10.1002/adem.201400147
- Y. Q. Qiao, J. P. Kong, X. P. Guo, Hot corrosion phenomena of Nb-Ti-Si based alloy and its silicide coating induced by different corrosive environments at 900 °C, *Ceram. Int.*, 44 (2018) 7, 7978–7990, doi:10.1016/j.ceramint.2018.01.238
- C. Vitelaru, N. Ghiban, A. C. Parau, M. Balaceanu, F. Miculescu, A. Vladescu, *Materialwiss. Werkstofftech.*, 45 (2014) 2, 91–98, doi:10.1002/mawe.201400191
- R. D. Liu, S. M. Jiang, H. J. Yu, J. Gong, C. Sun, Preparation and hot corrosion behaviour of Pt modified AlSiY coating on a Ni-based superalloy, *Corros. Sci.*, 104 (2016), 162–172, doi:10.1016/j.corsci.2015.12.007
- J. H. He, X. P. Guo, Y. Q. Qiao, Microstructure evolution and hot corrosion behavior of Zr-Y modified silicide coating prepared by two-step process, *Corros. Sci.*, 156 (2019), 44–57, doi:10.1016/j.corsci.2019.05.010
- J. R. Nicholls, J. Leggett, P. Andrews, Hot Salt Corrosion of titanium aluminides, *Mater. Corros.*, 48 (1997) 1, 56–64, doi:10.1002/maco.19970480110
- O. S. Kalakhan, Kinetic Regularities of the Electrochemical Processes of Corrosion Fatigue in Titanium Alloys, *Mater. Sci.*, 39 (2003) 5, 615–628, doi:10.1023/B:MASC.0000023500.42249.2b